Collagen and Leather

RESEARCH

Open Access

Guided bone regeneration in long-bone defect with a bilayer mineralized collagen membrane

Fuli Peng[1,2], Xuelei Zhang[3], Yilei Wang[2], Rui Zhao[4], Zhiwei Cao[5], Siyu Chen[2], Yunxuan Ruan[2], Jingjing Wu[6], Tianxi Song[6], Zhiye Qiu[6], Xiao Yang[2*], Yi Zeng[1*], Xiangdong Zhu[2], Jian Pan[5] and Xingdong Zhang[2]

Abstract

Bone regeneration for large, critical-sized bone defects remains a clinical challenge nowadays. Guided bone regeneration (GBR) is a promising technique for the repair of multiple bone defects, which is widely used in oral and maxillofacial bone defects but is still unsatisfied in the treatment of long bone defects. Here, we successfully fabricated a bilayer mineralized collagen/collagen (MC/Col)-GBR membrane with excellent osteoinductive and barrier function by coating the MC particles prepared via in situ biomimetic mineralization process on one side of a sheet-like pure collagen layer. The aim of the present study was to investigate the physicochemical properties and biological functions of the MC/Col film, and to further evaluate its bone regeneration efficiency in large bone defect repair. Fourier-transform infrared spectra and X-ray diffraction patterns confirmed the presence of both hydroxyapatite and collagen phase in the MC/Col film, as well as the chemical interaction between them. stereo microscope, scanning electron microscopy and atomic force microscope showed the uniform distribution of MC particles in the MC/Col film, resulting in a rougher surface compared to the pure Col film. The quantitative analysis of surface contact angle, light transmittance and tensile strength demonstrated that the MC/Col film have better hydrophilicity, mechanical properties, light-barrier properties, respectively. In vitro macrophage co-culture experiments showed that the MC/Col film can effectively inhibit macrophage proliferation and fusion, reducing fibrous capsule formation. In vivo bone repair assessment of a rabbit critical segmental radial defect proved that the MC/Col film performed better than other groups in promoting bone repair and regeneration due to their unique dual osteoinductive/barrier function. These findings provided evidence that MC/Col film has a great clinical potential for effective bone defect repair.

Keywords Mineralized collagen, Collagen, Guided bone regeneration, Artificial periosteum, Bone defect repair

*Correspondence:
Xiao Yang
xiaoyang114@foxmail.com
Yi Zeng
zengyi51@scu.edu.cn
Full list of author information is available at the end of the article

Graphic abstract

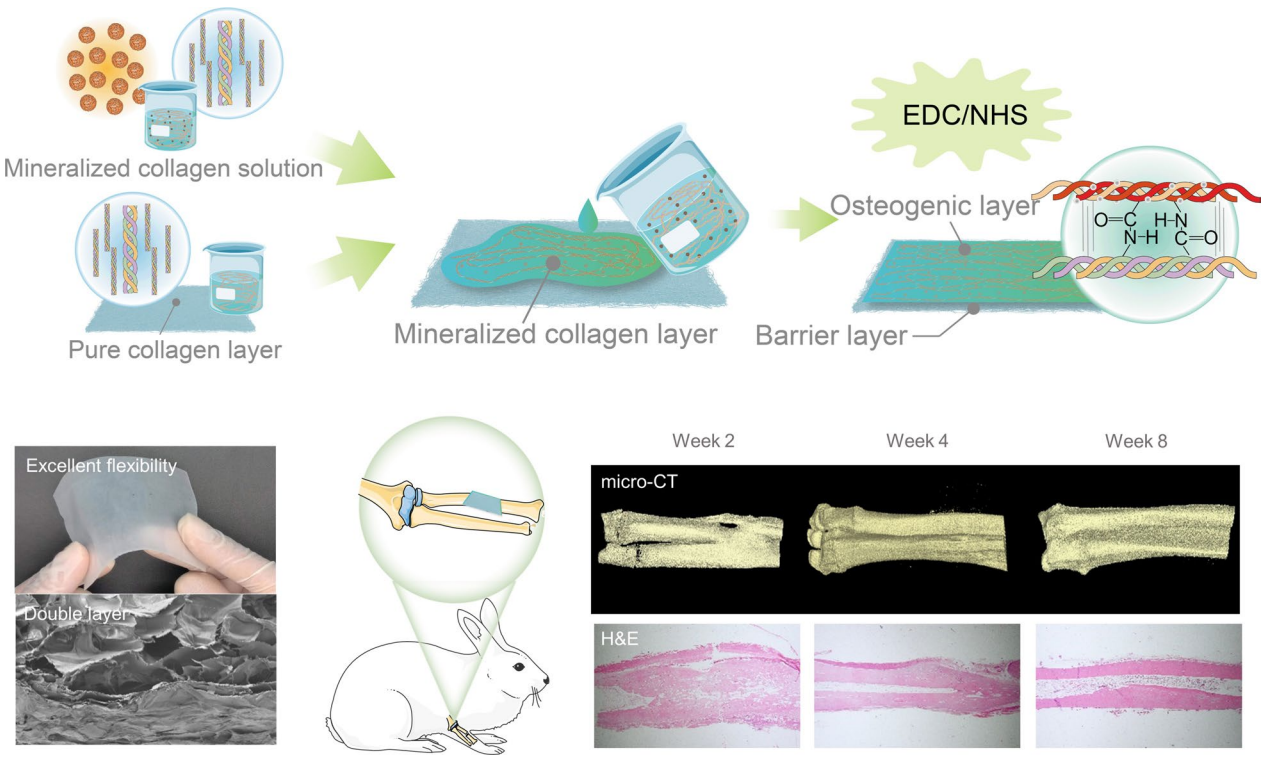

1 Introduction

Bone defect, often caused by trauma, disease, surgery, or congenital malformations, is a significant health problem worldwide, resulting in decreased life quality and increased healthcare costs. Its incidence is increasing due to the aging of the global population coupled with higher obesity ratio and insufficient physical activity of the working class [1]. It's estimated that there are approximately 20 million patients worldwide annually who suffer from a lack of bone tissue, with more than half a million in the United States and Europe, where the annual cost of treating bone defects is approximately greater than $5 billion [2, 3]. Bone regeneration for large critical-sized bone defects, referring to the defects longer than 1–3 cm with a loss of bone circumference of greater than 50%, presents a great clinical challenge in terms of non-union or delayed union [4]. Bone defect reconstruction can be achieved currently by different strategies including traditional bone-grafting procedures, which are usually carried out using four main categories of materials, i.e., autografts, allografts, xenografts, and biomaterial-based bone graft substitutes [5]. The techniques involved include distraction osteogenesis (the Ilizarov technique), induced membrane technique (the Masquelet technique), and vascularized fibular grafting (VFG) [5]. Among these, autologous bone grafting is considered the gold standard but is limited by severe complications, i.e., additional surgery, and the amount of tissue available (less desirable for segmental bone defects larger than 5 cm) [6, 7]. And the remaining strategies currently are also associated with their own complications and drawbacks to their application and availability. The emergence and development of guided bone regeneration provides a new clinical option. And the use of artificial periosteum as a barrier membrane in guided bone regeneration has attracted much interest from researchers [8].

Guided bone regeneration (GBR) was first proposed by Nyman et al. [9] in the 1980s, based on experiments investigating the healing of periodontal tissues. Subsequently, Buser et al. [10] developed the surgical procedures for GBR in 1990s, which made it possible for the technique to be used in oral and maxillofacial repair widely. Conventional barrier membrane materials used in GBR procedures can be grouped as non-bioabsorbable membranes (PTFE, Ti meshes) and bioabsorbable membranes (polylactide, collagen, and polyglycolide) [11]. These membranes act not only as a barrier to seal

off the defect from the surrounding soft tissue but also as a scaffold to promote the adhesion and proliferation of osteogenic precursor cells. However, compared to natural periosteum, the lack of adequate mechanical properties, degradation rates and osteoinductivity of the conventional GBR membranes limits their use in the treatment of large bone defects. The selection of appropriate materials to manufacture new generation bioactive GBR membranes is a critical stage in the development of the GBR technique.

As is known, collagen, the major organic component of bone tissue, has been the most commonly used artificial periosteum material as well as GBR membrane material due to its low immunogenicity and similar composition of natural periosteum. Collagen membranes are also preferred over other bioabsorbable membranes because of their hemostatic function, permeability (facilitating nutrient transport), and their superior ability to promote adhesion and growth of the osteogenic precursor cells [12]. Despite their advantages, collagen membranes have non-negligible drawbacks, such as relatively poor tensile stress bearing ability, low osteoconductivity, and an uncontrollable degradation profile by the ubiquitous collagen enzymes in vivo [13–16], which have impeded their application. Various studies have attempted to improve the properties of collagen membranes, including the addition of minerals to the collagen phase. A typical class of material is bone-like apatite, which has been widely used as the artificial bone material. Bone-like apatite, with the composition of calcium and phosphate, shows excellent biocompatibility and osteoinductivity [17–19]. Recent studies have demonstrated that the bone-like apatite/collagen composite materials potentially are useful for bone regeneration in bone defect repair. Among these, mineralized collagen (MC), a biomimetic composite of collagen and hydroxyapatite, stands out for its close chemical and structural resemblance to natural bone tissue [20, 21]. Until now, there are numerous MC-based bone substitute materials, some of which have been commercialized and approved by governmental administrations for clinical application [22]. Lian et al. [23] demonstrated that MC is a good autograft alternative in displaced intra-articular calcaneal fractures with trabecular defects. Kou et al. [24] showed an effective result of MC in the treatment of bone nonunion. Nevins et al. [25] observed that the use of MC combined with recombinant human platelet-derived growth factor-BB in extraction socket defects in patients would promote bone formation.

Here, we designed and prepared an artificial periosteum, defined as 'MC/Col film', which consists of a mineralized collagen layer with a rough surface and a pure collagen layer with a smooth surface. The MC particles used in this study were prepared according to a biomimetic mineralization process [26]. The design concept is that the mineralized collagen side of the MC/Col film can successfully promote osteoinduction for bone defect repair with high cytocompatibility, and the pure collagen side will exhibit good properties as a barrier to shield the local regenerative environment. In this study, together with the physicochemical and mechanical properties evaluation, we further investigated the bone regeneration ability of the MC/Col film to act as a GBR membrane using a segmental radial defect model in New Zealand white rabbits.

2 Materials and methods

2.1 Materials and chemicals

Ethylenediaminetetraacetic acid disodium salt (EDTA-2Na) was purchased from BioFROXX Co. (Einhausen, Germany). Sodium hydroxide (NaOH), anhydrous ethanol (EtOH), hydrochloric acid (HCl), dimethyl sulfoxide (DMSO), and other chemical reagents were supplied by Kelong Chemical Reagent Co. Ltd. (Chengdu, China). The cell culture reagents used in this study including 10% fetal bovine serum (FBS) and Dulbecco's Modified Eagle Medium (DMEM) (1% penicillin-streptomycin solution) were provided by Life Technologies Corp. (California, USA). Specimen handling reagents such as phosphate buffered saline (PBS, pH = 7.4), 4% polyformaldehyde, and other reagents such as 0.1% pentobarbital sodium, fluorescein diacetate (FDA), and 3-(4,5-dimethylthiazol-2-yl)-2,5-diphenyl-2*H*-tetrazol-3-ium bromide (MTT) were obtained from Sigma-Aldrich, Inc. (St. Louis, MO, USA). All of the above experimental reagents were applied without further purification.

2.2 Preparation of MC/Col film

The MC/Col film was prepared by the following two main steps and a schematic illustration of the fabrication process is shown in Fig. 1A.

Firstly, the biomimetic MC particles, as one of the most important ingredients, was prepared via the in situ biomimetic mineralization process according to a method our group reported previously [21, 27]. Type-I collagen fibrils extracted from the bovine achilles tendon were dissolved in acetic acid and stirred for more than 10 h to provide a homogeneous collagen solution. Water-soluble phosphate salt and calcium salt solution were added at a Ca/P molar ratio of 1.67 into the acidic collagen solution respectively under gentle magnetic stirring at room temperature, and then the pH value of the liquid mixture was adjusted to 8.0 with NaOH to form MC deposits. This step was similar to the biomineralization process of the natural bone. During this process, amorphous calcium phosphate precursors nucleated on the surface of

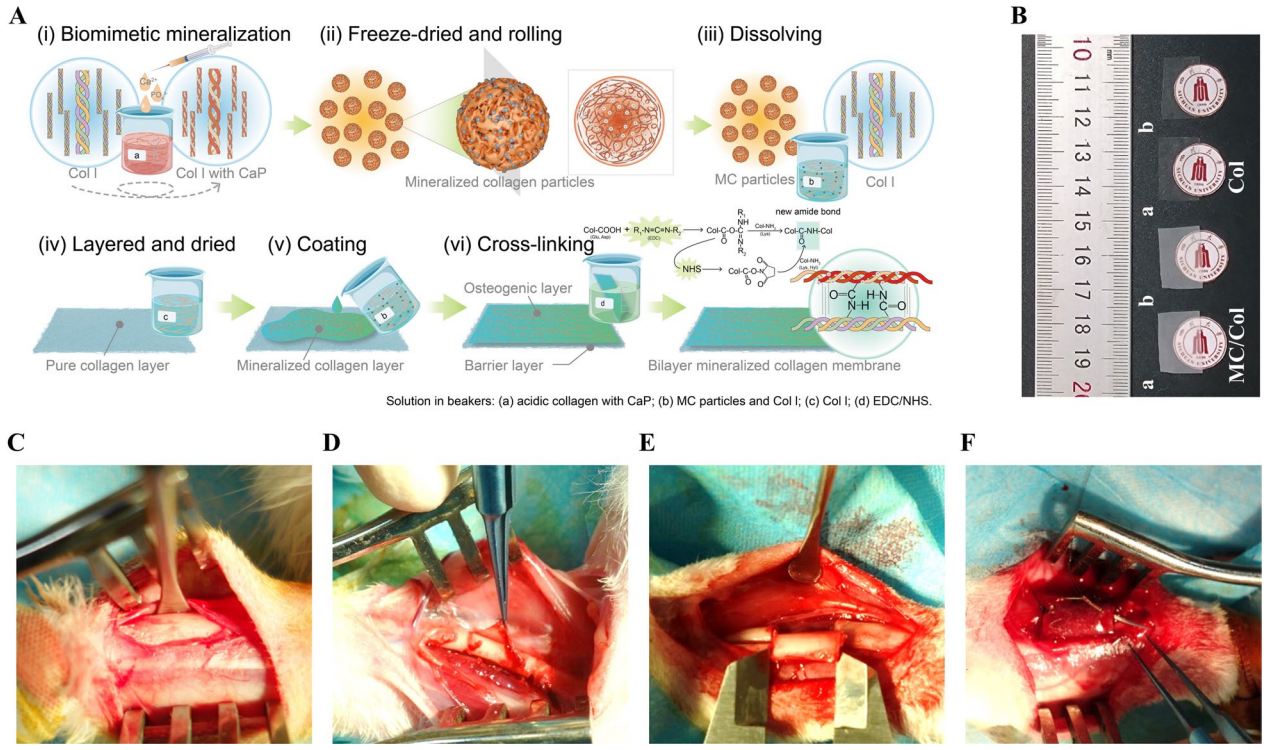

Fig. 1 **A** Preparation of the MC particles and MC/Col film. **B** Macroscopic morphology of the two sides (a, b) of the Col film, and the pure collagen side (a) and the mineralized collagen side (b) of the MC/Col film. **C**–**F** Animal surgical procedure to insert the artificial periosteum: The radial was exposed **C** and then peeled off the autogenous periosteum, leaving denuded bone below **D**. The denuded bone was osteotomized **E**, and the artificial periosteum was spread over the defect sites and sutured with the remaining autologous periosteum **F**

collagen microfibrils and were then converted to crystalline hydroxyapatite, with the crystallographic c-axis parallel to the collagen fibril length, guided by the collagen microfibrils [26, 28]. The deposits were washed with deionized water three times, and then freeze-dried to obtain porous MC particles. The obtained MC particles exhibited an interconnected porous microarchitecture, similar to our previous findings [29], aiming to facilitate the subsequent cellular infiltration and vascular penetration, and eventually an augmented bone regeneration.

Secondly, the MC/Col film composed of a barrier layer and osteogenic layer was built. The barrier layer, also defined as pure collagen layer, was synthesized by pure type-I collagen solution only. Briefly, 10 mL collagen solution was poured into PTFE mold evenly by rolling and dried in blast drying oven at 40 °C for 2 h. Meanwhile, the solution of the osteogenic layer also defined as mineralized collagen layer was made by adding 20% porous MC particles into 1% (W/W) type-I collagen gel and stirred thoroughly. Then, the osteogenic solution was poured on the pure collagen layer evenly and dried in blast drying oven for 24 h. For the better integration of two layers, the bilayer membrane was cross-linked by immersing in the EDC/NHS (100 mM:25 mM) solution in 90% alcohol at − 4 °C for 6 h, and then washed with ethanol and deionized water for 3 times respectively, and dried in vacuum oven for 24 h. The final product was sterilized by ^{60}Co radiation.

2.3 Characterization of MC/Col film

To determine the physicochemical and mechanical properties of the artificial periosteum, a pure collagen membrane recorded as 'Col film' provided by Allgens Medical Technology Co. Ltd. (Beijing, China) was used as a control in all experiments. Unless otherwise noted, the test of the MC/Col film was performed on the mineralized collagen side.

2.3.1 Structure identification

The chemical structure of the Col and MC/Col films were studied by Fourier-transform infrared (FT-IR) spectra taken on an INVENIO™ Fourier-transform infrared spectroscopy (Bruker, Germany). The spectra were collected at the scanning wavenumber ranges from 700 to 4000 cm^{-1}. Further, the phase composition and crystal structure of the Col and MC/Col films were investigated via X-ray diffraction (XRD) patterns obtained

on an Empyrean X-ray diffractometer (PANalytical, Netherlands).

2.3.2 Morphology observation

The surface morphology of the Col and MC/Col films was visually characterized by a stereo microscope (SM, Olympus, Japan) and a field-emission scanning electron microscopy (SEM, Hitachi S-4800, Japan) under different multiples. Before the SEM observation, all samples were sprayed with gold for 90 s. The elemental composition and distribution of samples were conducted by the scanning electron microscopy equipped with an energy-dispersive spectrum (EDS, Hitachi S-4800, Japan). In addition, the surface roughness of the samples was examined by a Dimension ICON atomic force microscope (AFM, Bruker, Germany) instrument. NanoScope analysis (version 2.00) was used to analyze the images and calculate roughness parameter from the scanned area.

2.3.3 Surface hydrophilicity and optical properties

The surface wettability of the Col and MC/Col films were analyzed by surface contact angle (SCA) measured through a Theta water contact angle tester (Biolin, Sweden). 10 μL distilled water was used as the indicator, and at least four different points of each sample were tested.

The optical properties of the Col and MC/Col films were evaluated by the light transmittance of dried films at the wavelength from 200 to 800 nm, using an UV–Vis spectrophotometer (UV-2600, Hitachi, Japan) according to ASTM method D1746-15 [30]. Based on Beer–Lambert's law, the light transmittance was calculated as follows [31].

$$\text{Light transmittance } (\%) = \frac{1}{10^{\text{OD}}} \times 100\%$$

where OD is the absorbance at selected wavelengths.

2.3.4 Mechanical properties

The mechanical properties of the Col and MC/Col films were investigated by the bending and tensile test. The bending test was performed on dry film samples to evaluate the flexibility and good resistance to cracking of samples, while the tensile test was accomplished under both wet and dry conditions using a universal testing machine (UTM, Shimadzu, Japan) to evaluate the tensile strength of samples. For wet state tensile test, the films were immersed into deionized water at 25 °C for 2 min prior to the test [32]. At least three specimens of each sample were tested under each condition to obtain the average value of tensile strength.

2.4 In vitro macrophage co-culture

Mouse RAW 264.7 macrophages were purchased from Chinese Academy of Sciences (Shanghai, China). The prepared samples of the Col and MC/Col films were placed in cell culture plates. The cells were then seeded at a density of 1×10^5 cells per well and cultured in Dulbecco's Modified Eagle Medium (DMEM) supplemented with 10% FBS and 1% penicillin-streptomycin cocktail in an incubator under an atmosphere of 5% CO_2 at 37 °C. It has to be mentioned that the RAW 264.7 macrophages were seeded on the mineralized collagen side of the MC/Col film. Cell live/dead fluorescent staining, MTT assays, and cell morphology experiments were performed on days 1, 4, and 7.

2.4.1 Cell viability and proliferation

To test the survival and proliferation of the macrophages on the surface of samples, live/dead fluorescent staining and MTT assays were performed on days 1, 4 and 7. For live/dead assays, the cells were gently rinsed several times with PBS, followed by staining with live/dead dye (FDA/PI) in the dark until the cells were stained. Cell viability was then observed by a confocal laser scanning microscopy (CLSM, Carl Zeiss, Germany). For MTT assays, after removing the excess of culture medium with PBS, 100 μL MTT solution (5 mg/mL) was introduced to each well and incubated with the cells for 4 h at 37 °C in the dark. After incubation for 4 h, DMSO was added to dissolve the blue thyroxine crystals and the optical density (OD) of the resulting solutions was measured under the wavelength of 570 nm using a Synergy H1 multifunctional enzyme marker (BioTek, USA).

2.4.2 Cell morphology

To evaluate cell morphology, TRITC-phalloidin and 4′,6-diamidino-2-phenylindole (DAPI) were used for the cytoskeletal F-actin and nuclear staining, respectively. In brief, on days 1, 4 and 7, macrophages were fixed with 4% paraformaldehyde, and stained with TRITC-phalloidin for 30 min, followed by counterstaining with DAPI. To investigate the effect of the Col and MC/Col films on macrophage fusion competency, the expression of cells fusion protein genes, CD44, CD47 and DC-STAMP, was studied. Cell culture on days 1, 4 and 7 was collected for analysis of fusion-related gene expressions with qPCR. The total RNA from different groups were extracted by a RNeasy Mini Kit (Qiagen, Germany) and were then reverse transcribed into complementary DNA (cDNA) using an iScript™ cDNA Synthesis Kit (Bio-Rad, CA, USA). Real-time quantitative PCR reaction was performed using SoFast™ EvaGreen® Supermix (Bio-Rad, USA). Subsequently, the expression levels of CD44, CD47 and DC-STAMP were measured and analyzed.

2.5 Evaluation of in vivo radial bone defect repair in rabbit model

2.5.1 Animal surgery

To evaluate the bone regeneration efficiency of the fabricated artificial periosteum, bilateral large segmental radial defect model in adult rabbits was employed in this current work. All experimental procedures performed were approved by the Institutional Animal Care and Use Committee (IACUC) of Sichuan University and followed the Guidelines for Care and Use of Laboratory Animals of Sichuan University.

The experimental design was as follows, and the surgical procedure was shown in the Fig. 1C–F. 12-week-old New Zealand white rabbits were purchased from Experimental Animal Center of Sichuan University (Chengdu, China). To prepare for surgery, the weighed rabbits were anesthetized with 2–3% isoflurane using an anesthesia machine and kept at a horizontal position, then the surgical areas of bilateral forelimbs were shaved and sterilized by iodine. Bilateral radials and attached periosteum were exposed through a lateral longitudinal skin incision followed by separation of the skin, fascia and muscles of the forearm. Subsequently, the periosteum was peeled carefully, and a segmental defect of 10 mm was created in the middle of radial bone using a hemostat. Twenty-four bone defects in bilateral radials in 12 rabbits were randomly divided into 3 groups with 8 defects for each group: (1) control group (without treatment), (2) Col group (treated with the Col film), (3) MC/Col group (treated with the MC/Col film). Specifically, the film materials from the Col and MC/Col groups were spread over the defect sites, wrapped tightly to both bone ends of defects, and sutured with the remaining autologous periosteum on both sides. Notably, the mineralized collagen side of the MC/Col film was placed toward the defect site. Internal fixation of the osteotomized radial was unnecessary because the ulna can act as external fixation to support the forelimb through the interosseous membrane and ligaments [33–35]. After implantation, the tissues were then sutured in layers. At weeks 2, 4 and 8 after surgery, the rabbits were euthanized using an overdose of pentobarbital, and complete forelimb samples (including radial and ulna) were harvested and fixed in 4% paraformaldehyde for further analysis.

2.5.2 Micro-computed tomography (micro-CT) examination

To assess the amount of new bone within the defect area, a high-resolution micro-CT system (μ-CT, Scanco Medical, Switzerland) was performed at weeks 2, 4 and 8. The harvested specimens were scanned at an energy level of 70 kV, an intensity of 114 μA, and a pixel matrix of 2048 × 2048. After scanning, the resulting greyscale images were analyzed and reconstructed using Mimics Research 17.0 (Materializ, Belgium) to provide a three-dimensional model, and the areas of new bone formation in the defects were quantified through threshold partition and Boolean calculation. The region of interest was a three-dimensional volume that extends over the entire 10-mm radial defect space created at the time of surgery. Quantitative data such as bone mineral density (BMD) were then obtained. The morphology of the regenerated bone at week 8 after surgery was also assessed by radiographic analysis. The X-ray radiographs of rabbit forelimb specimens were taken using a Siemens digital X-ray machine (Germany).

2.5.3 Histological analyses

After micro-CT analysis, all fixed specimens were decalcified in 20% neutral phosphate-buffered EDTA solution for approximately 1 month at room temperature. Half of the ulna of each specimen was then removed along the sagittal direction. The remainder of each specimen was dehydrated in a series of ethanol (70 to 100%), embedded in paraffin, and sliced into 5-μm section. After routine histological preparation, the tissue sections were stained with hematoxylin and eosin (H&E) or Masson's trichrome, followed by observation using a Pannoramic MIDI pathological section scanner (Budapest, Hungary).

2.6 Statistical analyses

All quantitative data collected from at least three independent trials per experiment were presented as the mean ± standard deviation (SD). Statistical analyses were performed using Microsoft Office Excel 2021 and OriginPro 2023b SR1. Significant differences among groups were indicated by student's t test or one-way analysis followed by post-hoc Tukey's test, and the differences between groups of $^{*}p < 0.05$, $^{**}p < 0.01$, $^{***}p < 0.001$ and $^{****}p < 0.0001$ were considered significant, while *ns* was defined as not significant ($p > 0.05$).

3 Results and discussion

Healing of large bone defects requires operative intervention and remains a significant clinical problem. A main obstacle for successful bone regeneration and bone healing is the rapid formation of connective tissue at the bone defect area, in contrast to osteogenesis [36–38]. Therefore, the GBR technique has attracted considerable attention in recent years due to its principle of preventing connective tissue invasion into the defect. The membrane plays a vital role in the GBR technique, acting not only as a barrier to seal off the defect from the surrounding soft tissue, but also as a scaffold to promote the adhesion and proliferation of osteogenic precursor cells. It has been proposed that an ideal GBR membrane should address the requirements for biocompatibility, cell-occlusiveness,

space maintaining capacity, tissue integration, and clinical manageability [39]. In the current study, we prepared a novel artificial periosteum with excellent dual osteoinductive and barrier function as a GBR membrane in bone defect repair. We further demonstrated its potential effects to fully repair large bone defects, providing new intriguing cues for the clinical application of the GBR technique in segmental bone defect repair.

3.1 Characterization of MC/Col film

3.1.1 Structure identification

FT-IR spectra were used to confirm the structure of the MC/Col film and to verify the structural differences between the Col film and MC/Col film. As shown in Fig. 2E, the infrared spectrum of the MC/Col film showed the PO_4^{3-} band (1031 cm^{-1}) consistent with the standard patterns of hydroxyapatite and the characteristic bands of collagen, such as amide A (3332 cm^{-1}), amide I (1637 cm^{-1}), amide II (1528 cm^{-1}) and amide III (1224 cm^{-1}) [40, 41]. The absorption peak of amide A (3332 cm^{-1}) is N–H stretching vibration, whose frequency depends on the strength of the hydrogen bond between the collagen chains. The peaks of amide I (1637 cm^{-1}), amide II (1528 cm^{-1}) and amide III (1224 cm^{-1}) corresponded to C=O stretching vibration, the out-of-phase combination of N–H bending vibration and the C–N stretching vibration, and N–H bending vibration, respectively, were weakened in the MC/Col film compared with the Col film, indicating that the binding of hydroxyapatite to collagen fibers has successfully occurred. Moreover, the presence of these amide bands further revealed that the triple helix structure of collagen was maintained in the MC/Col film, consistent with the Col film [42].

For further confirmation of the presence of hydroxyapatite in the MC/Col film, the phase composition of the Col and MC/Col films were identified by XRD analysis. As shown in Fig. 2F, the diffraction patterns of the Col and MC/Col films presented similar amorphous hump-like peaks at $2\theta = 8°$ and 22° [43]. However, compared to the Col film, the corresponding characteristic peaks of the MC/Col film are attenuated, which was due to the presence of the MC particles coating on the MC/Col film. Furthermore, the pattern of the MC/Col film contained some typical but broader and weaker HA diffraction peaks of (002), (211), (300), (202), (310), (213) and (004), implying that the deposited hydroxyapatite minerals via biomimetic mineralization process with poor crystallinity in the composite similar to that of the regenerated bone tissue, resulting in greater absorption in vivo [44–46]. The XRD results were in agreement with the FT-IR results, indicating that the MC/Col film contained both hydroxyapatite and collagen phases.

3.1.2 Morphology observation

The macro-appearance of the Col film was transparent and homogeneous, whereas the MC/Col film appeared as a white sheet, as shown in Fig. 1B. SM and SEM images were used to visualize the surface morphology of the samples and the homogeneity of MC particles loading inside the MC/Col film. Based on the SM images shown in Fig. 2A, the surface of the Col film was smoother, and the ridged surface protrusions are suspected to be collagen fibers, which were arranged in a network and the woven structure was dense. Compared to the Col film, certain irregular MC particles with a darker color appeared to be homogeneously distributed within the MC/Col film with average sizes ranging from 10 to 100 μm. The closer to the surface, the larger the particle size of MC particles. The gravity of the MC particles during the manufacturing process contributed to their spatial distribution.

A similar result was seen more evidently in the SEM images (Fig. 2C), that is, the MC/Col film exhibited certain granular aggregates of a narrow range of size with a clear boundary in addition to relatively loose ridged protrusions, while the Col film was relatively flat and there were only denser ridged protrusions with blurred boundaries on the surface. Larger magnification revealed that the MC particles on the surface of the MC/Col film were almost completely covered by a thin layer of collagen, which prevented the unnecessary loss of MC particles due to friction or extrusion during surgery. The distribution situation of chemical elements in the samples was investigated by EDS analysis. From the EDS mapping inserted in Fig. 2C, it can be visualized that the main chemical elements of the MC/Col film are calcium (Ca), phosphate (P), carbon (C) and oxygen (O) elements, whereas the Col film contains only carbon (C) and oxygen (O) elements, confirming the occurrence of collagen mineralization. Besides, as can be seen in the cross-sectional SEM micrographs in Fig. 2D, the MC/Col film presented two distinct layers: a dense layer, composed of collagen, which directly contacts with the surface of the soft tissue and is beneficial in preventing the fibrous connective tissue from growing into the defected region; and a loose layer, composed of MC particles and collagen, which directly contacts with the surface of the defected bone tissue and provides an ideal environment for osteoblasts to grow and proliferate. The whole thickness of the MC/Col film was approximately 0.6 mm, which facilitates surgical manipulation and provides appropriate mechanical strength and biodegradation period for GBR.

AFM analysis was used to examine the 3D surface topography and measure the surface roughness of the samples. In Fig. 3A, the three-dimensional (3D) AFM images of the Col and MC/Col films can be observed. The arithmetic average (Ra) of the surface and the

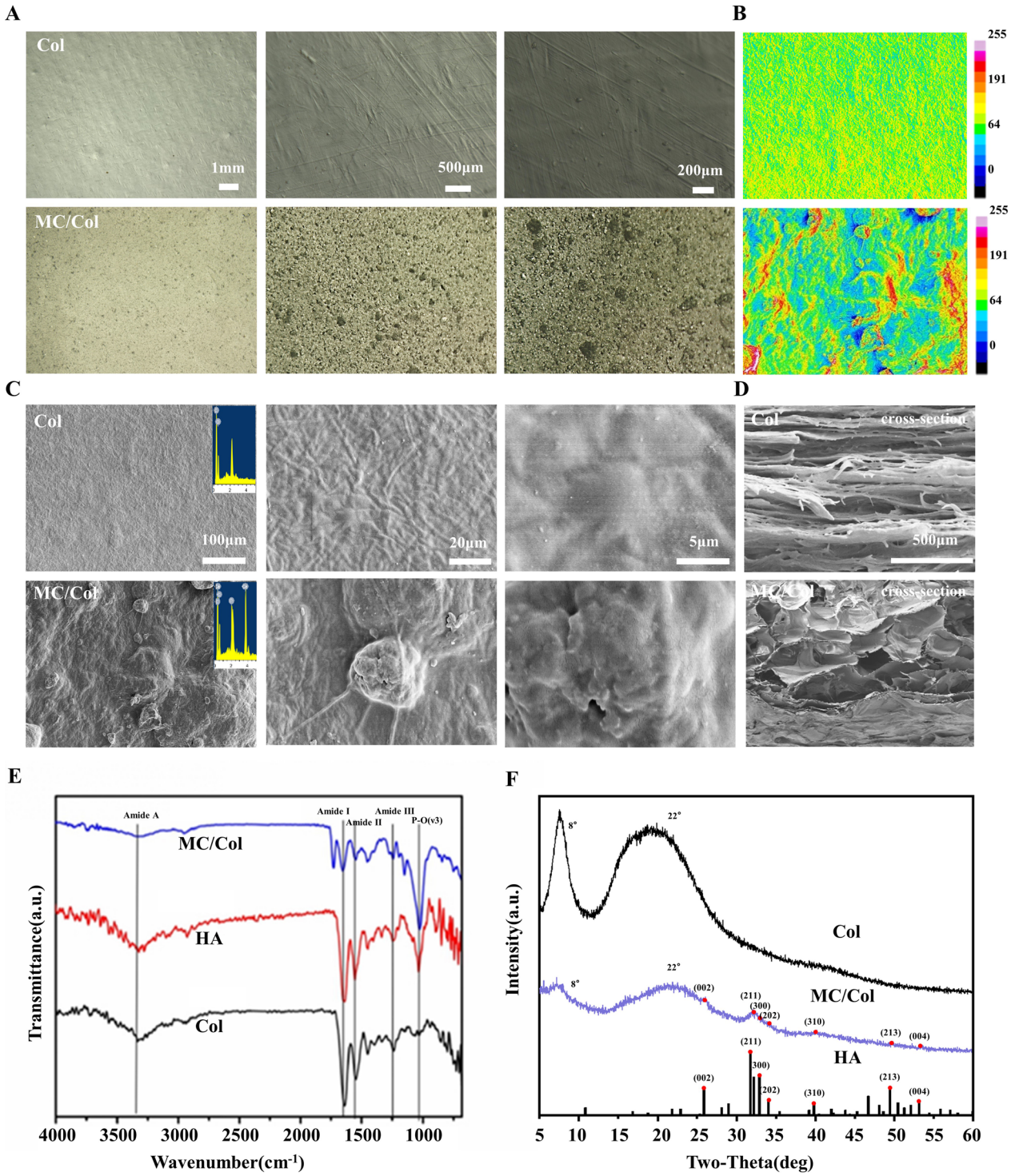

Fig. 2 **A** SM images of the Col and MC/Col films with ×7.5, ×25 and ×100 magnifications and the respective SEM pseudo-colored images **B**. **C**, **D** SEM images of the surface (with an additional EDS image on the right upper) with ×1000, ×5000 and ×20,000 magnifications and cross-sections of the two films, respectively. **E** FT-IR spectra of the hydroxyapatite, Col and MC/Col films. **F** XRD patterns of the Col and MC/Col films. Standard Spectrum of hydroxyapatite was provided below

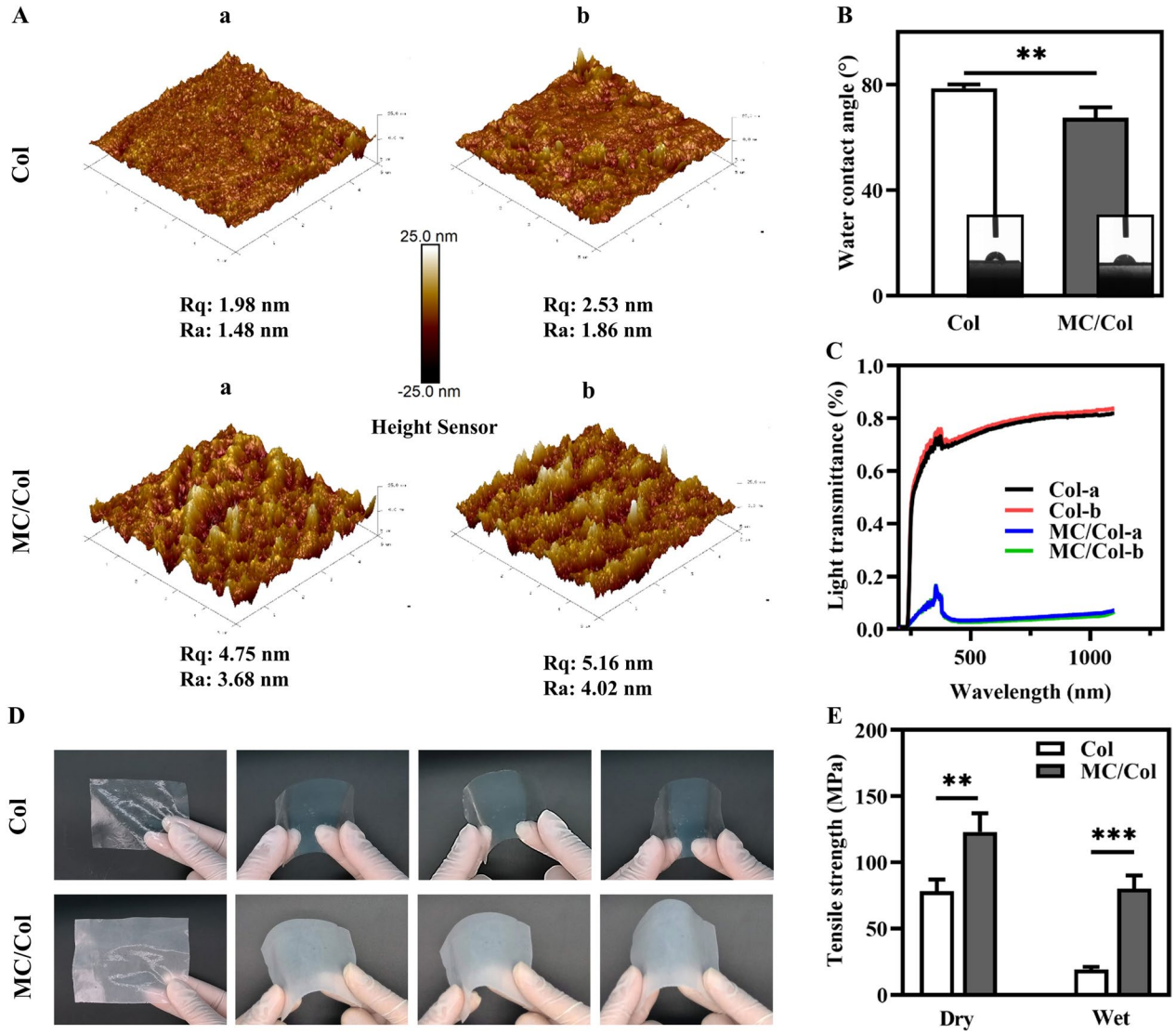

Fig. 3 **A** AFM images (5 μm×5 μm) of the two sides (a, b) of the Col film, and the pure collagen side (a) and the mineralized collagen side (b) of the MC/Col film. **B**, **C** The water contact angle and light transmittance of the two films, respectively. **D** In situ bending test, series of morphology images with the bending process of the two films. **E** Dry and wet tensile strength of the two films. (*$p < 0.05$, **$p < 0.01$, ***$p < 0.001$, ****$p < 0.0001$. All the data are reported as mean ± standard error.)

root-mean-square average (Rq) of height deviations for Col film were determined to be 1.48 and 1.98 nm on one side (a-side) and 1.86 and 2.53 nm on the other side (b-side), respectively, whereas the Ra value and Rq value for MC/Col film were 3.68 and 4.75 nm on the pure collagen side (a-side) and 4.02 and 5.16 nm on the mineralized collagen side (b-side), respectively. After mineralization, the roughness of the film increased slightly, indicating that the good hydrogen bonding interaction between the hydroxyl group of hydroxyapatite and the carboxyl group of collagen leads to a uniform distribution of MC particles in the collagen matrix.

All together, these results showed that the MC particles was efficiently loaded onto the surface of the MC/Col film designed for bone regeneration.

3.1.3 Surface hydrophilicity and optical properties

Surface contact angle measured by the static sessile drop method was used to evaluate the hydrophilicity of the samples, which is associated with cell adhesion and proliferation. Based on the images presented in Fig. 3B, the contact angle of the MC/Col film (67.45°)

was significantly lower than that of the Col film (78.73°) ($p < 0.05$). This result indicated that the wettability of the MC/Col film was improved due to the large number of hydrophilic hydroxyl groups provided by hydroxyapatite.

Light transmittance was used to evaluate the light barrier properties of the Col and MC/Col films, which is essential to a film's function-ability. The transmission of the two samples at selected wavelength (200–800 nm) were shown in Fig. 3C. In the UV–Vis range, the MC/Col film blocked at least 80% of UV light transmission and almost all visible light transmission, while the Col film blocked less than 30% of the UV light transmission and less than 20% of the visible light transmission. The increased light-barrier property of the artificial periosteum was due to the effective scattering and reflection of UV–visible light by the MC particles that were loaded onto the film [47].

3.1.4 Mechanical properties

An obvious drawback of current available artificial periosteum on market is that it is difficult to effectively anchor or integrate with bone scaffolds, which will lead to serious complications in clinical procedures [48]. Therefore, it is important to take flexibility into account in the preparation of an artificial periosteum. For example, a recent study demonstrated that 2D ultrathin polymeric nanosheets were ideal candidates for artificial periosteum due to their unique feature of flexibility [48]. In this study, both of the Col film and the MC/Col film exhibited excellent flexibility, which facilitates suture manipulation during surgery, and good resistance to cracking, which helps maintain the functional integrity of films, as demonstrated by their bending tests (Fig. 3D). There were no visible cracks in the two groups, even when the bending angle was gradually increased.

The tensile strength was used to further investigate the mechanical properties of the Col and MC/Col films. Notably, the mechanical properties of artificial bone membrane samples under wet conditions, closely related to clinical application, have been neglected in most studies, which have mainly focused on the mechanical properties of dry samples [49]. Here, we measured the tensile strength of samples under both dry and wet conditions simultaneously. The average tensile strengths of the dry and wet Col film were 78 ± 9 MPa and 19 ± 2 MPa, respectively, while that of the corresponding MC/Col film were 123 ± 14 MPa and 80 ± 10 MPa, respectively. As expected, the MC/Col film in dry or wet state all showed a significant increase in tensile strength in comparison with the control one ($p < 0.05$), as shown in Fig. 3E. This proved that minerals in the fabricated artificial periosteum should contribute to the general mechanical feature of the MC/Col film [50]. Besides, the cross-linking treatment also improved the thermal stability and tensile strength of the MC/Col film [51], in addition to enabling better integration.

3.2 In vitro macrophage co-culture

It is widely accepted that biomaterial-bone integration requires consideration of not only the osteoinductive properties of the biomaterials, but also the effect of the biomaterials on inflammation, which plays a critical role in the initializing process of implantation [52, 53]. The effects of MC particles on promoting osteogenic differentiation of human mesenchymal stem cells (hMSCs) have been demonstrated by many in vitro studies, and the related molecular mechanism at gene level has also been clarified [22, 54]. However, there are few reports on how MC particles affect the inflammatory response. Generally, physiologic inflammation contributes to the later neovascularization as well as osteogenic differentiation, but long-term or severe inflammation may lead to fibrous package tissue destruction, and even biomaterial-bone disruption [55–57].

It is generally known that monocytes/macrophages act as a switch that controls the body's inflammatory response [52]. Moreover, Gretzer et al. [58] demonstrated that fibrosis and encapsulation of the biomaterials always correlated with the macrophage density and fusion. Besides, Lee et al. [59] reported that the biocompatibility of the implant surface negatively associated with the density of macrophages. Thus, in this study, in vitro cell experiments were conducted using RAW 264.7 macrophages co-cultured on the surface of the Col and MC/Col films to investigate the potential inflammatory response of fabricated artificial periosteum.

3.2.1 Cell viability and proliferation

Cell live/dead fluorescent staining results were shown in Fig. 4A. Apparently, relatively fewer live cells, as stained in green, can be observed on the surface of the MC/Col film, whereas more dead cells, as stained in red, were presented on the surface compared to the Col film. This results of MTT assays were consistent with the Cell live/dead fluorescent staining study. Based on the proliferation data shown in Fig. 4B, the absorbance at 570 nm of the two groups increased on days 1, 4 and 7 consistently, indicating that macrophages could proliferate in a time-dependent manner in all groups, but the proliferation rate of macrophages on the MC/Col film was significantly lower than that on the Col film ($p < 0.05$). These results showed that the viability and proliferation of macrophages were inhibited by the MC/Col film. Similar observations have reported by Meng et al. [60] who found that macrophage cell proliferation was more

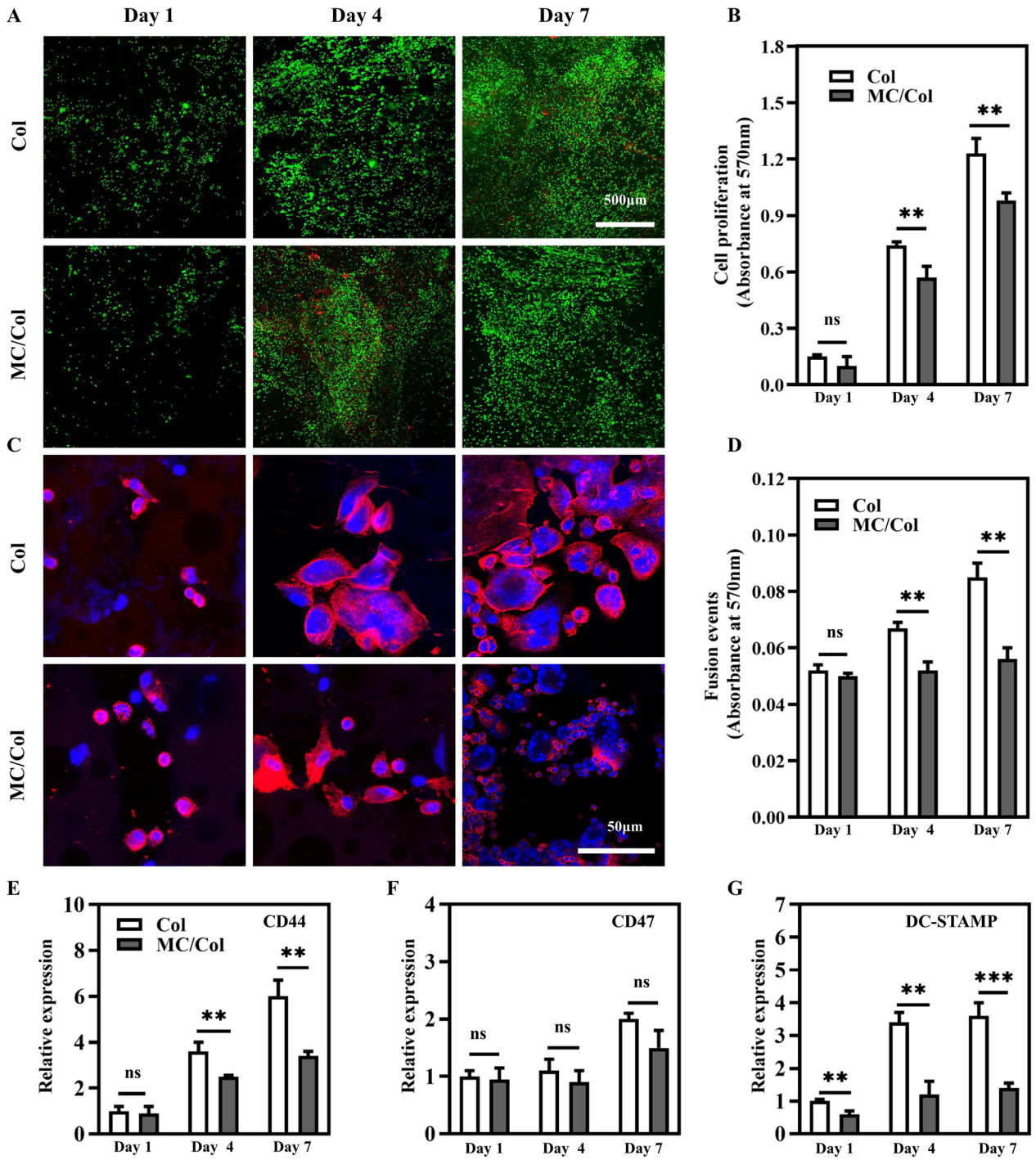

Fig. 4 Confocal laser scanning microscopy (CLSM) observations of live/dead cells (green/red) **A** MTT assays **B** nuclei/actin skeleton (blue/red) **C** fusion events **D** and qRT-PCR analysis of the gene expression levels of macrophage fusion related genes (CD44, CD47 and DC-STAMP) **E**, **F** and **G** of MSCs growth on the Col and MC/Col films on days 1, 4 and 7, respectively (*$p < 0.05$, **$p < 0.01$, ***$p < 0.001$, ****$p < 0.0001$. All the data are reported as mean ± standard error)

inhibited in the MC group than in the Col group on days 1 and 2.

3.2.2 Cell morphology

Recent studies have shown that inhibition of macrophage recruitment and fusion is related with reduced

thickness of the fiber capsule and improve the survival of the implants [58, 61, 62]. The actin cytoskeleton staining results were shown in Fig. 4C. The macrophages adhering to the surface of the Col film appeared in oval or spindle shape with more amoeboid-like protrusions, whereas macrophages on the MC/Col film had a rounder morphology. Besides, the number of multinucleated giant cells was significantly higher in the Col group than in the MC/Col group. Quantitative analysis of macrophage fusion also showed the same results, suggesting the fewer occurrence of cell fusion events in the MC/Col group ($p < 0.05$), as shown in Fig. 4D. Similar to our study, Shi et al. indicated that adhering to MC had a rounder morphology than those grown on culture glass [52]. The qPCR analysis of the gene expression levels of CD44, CD47 and DC-STAMP on days 1, 4 and 7 were shown in Fig. 4E–G, respectively. We found that gene expression levels of CD44, CD47 and DC-STAMP in both groups increased progressively with the prolonged culture time. There is no significant difference in the growth rate of CD47 expression among groups, but the growth rate of CD44 and DC-STAMP expression were significantly slower in the MC/Col group compared to the Col group at weeks 4 and 7. This indicated that the MC/Col film may affect the macrophage fusion by inhibiting the gene expression of CD44 and DC-STAMP. Recently, Fang et al. [63] in their study of the effect of three-dimensional matrices on macrophage fusion found that the stiffness of the three-dimensional matrix controlled the number of fused macrophages by altering the expression of these fusion proteins.

Results from in vitro cell experiments showed that the MC/Col film can effectively inhibit macrophage proliferation and fusion, reducing host rejection, excessive inflammatory response and fibrous capsule formation.

3.3 Evaluation of in vivo radial bone defect repair in rabbit model

While GBR is widely used in oral and maxillofacial reconstruction, its application in segmental defects is limited [64]. In this study, a 10-mm-segmental long-bone defect model in the rabbit radial was used in vivo studies of bone regeneration. As bone defect model is concerned, the radial was chosen because it is easily accessible, and does not require the introduction of additional internal fixation, which would increase trauma and experimental variability [35]. Besides, considering that no osteoinductive cytokines were introduced in the fabricated artificial periosteum, we used a 10-mm rather than 15-mm defect model, which is considered as the standard critical-size defect model of a rabbit's radial, to better characterize the osteoconductivity of the artificial periosteum. Zhou et al. demonstrated that a 10-mm radial defect in rabbits retained its size for 12 weeks after removal of the periosteum [65–67]. Similar to our study, Guda et al. [64] chose a healing 10-mm bone defect model rather than the more challenging 20-mm bone defect model when investigating the effect of combining hydroxyapatite scaffolds and collagen GBS membranes on bone regeneration in long bone defects for similar reasons.

3.3.1 Micro-computed tomography (micro-CT) examination

The representative 3D reconstructed micro-CT images of the rabbit forearm conducted at weeks 2, 4 and 8 were shown in Fig. 5A. The control group showed only minor new bone formation until 8 weeks. Compared with the control group, more new bone formation was present in the Col and MC/Col groups throughout the process. Both the Col and MC/Col groups exhibited comparatively good bridging and fast healing, but the MC/Col group performed better than the Col group with clearer boundary between ulna and repaired radius at week 8. In addition, the X-ray radiographs of these three groups at week 8 demonstrated a similar result. As shown in Fig. 5B, it can be distinctly observed that the defect in the MC/Col group has been completely covered by a robust callus with the formation of a uniform marrow cavity, and the defect in the Col group has been covered by a callus with partial marrow remodeling, whereas in the control group, at week 8, callus formation was noticed adjacent the construct but did not bridge the gap with the characteristics of a non-union. Our findings are consistent with the study conducted by Chen et al. [68], who found that the Col/HA scaffold group and SDF-1α/Col/HA scaffold group both exhibited comparatively good bridging and fast healing at week 8 in their study of matrix elasticity-modified scaffolds loaded with SDF-1α to improve in situ regeneration of radial segmental bone defects. They also found that the Col/HA scaffold group exhibited good MSC recruitment, which contributed to new bone formation. Further quantitative analysis of BMD within the 10-mm defect site allowed for a more accurate assessment of new bone formation within the osteotomy gap, and the results were shown in Fig. 5C. BMD increased in all three groups and was significantly higher in the MC/Col group than in the Col and the control groups from 2 to 8 weeks ($p < 0.05$).

These results suggested that the MC/Col group exhibited the optimal bone regeneration ability.

3.3.2 Histological analyses

Radiographic analysis and μ-CT analysis of the segmental defects were further supported by histological observation. The H&E staining and Masson trichrome staining

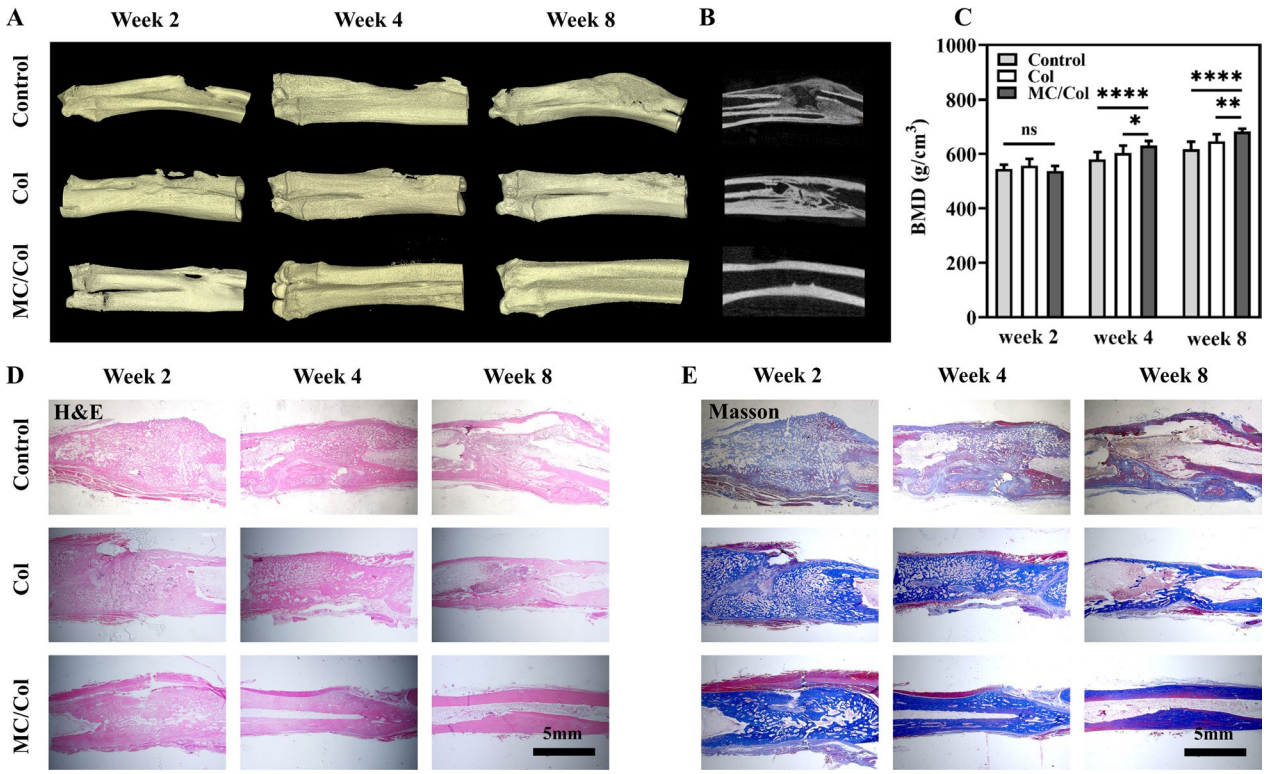

Fig. 5 **A** Three-dimensional reconstructed micro-CT images of rabbit radius defect model in the groups of the control, Col and MC/Col at weeks 2, 4 and 8. **B** The X-ray radiographs of rabbit radius defect model in different groups at week 8. **C** Quantitative micro-CT analysis of BMD (bone mineral density) in different groups at weeks 2, 4 and 8. **D**, **E** Hematoxylin–eosin (H&E) and Masson staining in different groups at weeks 2, 4 and 8, respectively. (*$p < 0.05$, **$p < 0.01$, ***$p < 0.001$, ****$p < 0.0001$. All the data are reported as mean ± standard error.)

images were shown in Fig. 5D and E. The control group showed massive fibrous tissue in the defect and essentially no mature new bone formation until 8 weeks after surgery. Compared to the control group, the Col and Col/HA groups had more pronounced new bone formation from 2 to 8 weeks, whereas the volume of newly formed bone tissue appeared to be greater in the Col/HA group at week 4, and mature trabecular and lamellar bone appeared to be more compact in the Col/HA group at week 8 [69, 70]. This further demonstrated that the MC/Col film exhibited better bone healing performances compared to the pure Col film, and possessed great capability to regenerate new bone of the defected region.

4 Conclusion

Taken together, we successfully fabricated and characterized the MC/Col film, a new bilayer mineralized GBR membrane consisting of an osteogenic layer and a barrier layer, which correspond to the mineralized collagen layer and the pure collagen layer, respectively. The chemical composition and microstructure of the MC/Col film were similar to that of natural periosteum, which facilitated the adhesion and proliferation of osteogenic precursor cells. In vitro experiments showed that the MC/Col film can effectively inhibit macrophage proliferation and fusion, reducing fibrous capsule formation. In vivo experiments demonstrated that the MC/Col film can prevent the defects from the surrounding soft tissue while promoting osteogenesis to repair the large segmental radial defect in rabbits. These results indicated that the MC/Col film possessed great potential for clinical applications of large bone defect repair.

Abbreviations

AFM	Atomic force microscopy
BMD	Bone mineral density
Col	Collagen
DAPI	4′,6-Diamidino-2-phenylindole
DMEM	Dulbecco's modified eagle medium
EDTA	Ethylenediaminetetraacetic acid
EDS	Energy-dispersive spectrum
FDA	Fluorescein diacetate
FBS	Fetal bovine serum
FT-IR	Fourier-transform infrared

GBR	Guided bone regeneration
H&E	Hematoxylin and eosin
MC	Mineralized collagen
MTT	3-(4,5-Dimethylthiazol-2-yl)-2,5-diphenyl-2 H-tetrazol-3-ium bromide
PBS	Phosphate buffered saline
SEM	Scanning electron microscopy
SM	Stereo microscope
SCA	Surface contact angle
UTM	Universal testing machine
VFG	Vascularized fibular grafting
XRD	X-ray diffraction

Acknowledgements
The authors are grateful to Li Chen from the Analytical & Testing Center of Sichuan University for her help of micro-CT images and Lingzhu Yu from the National Engineering Research Center for Biomaterials of Sichuan University for her help of SEM images.

Author contributions
FLP: Data curation, formal analysis, investigation, writing—original draft; XLZ: Methodology, visualization; YLW: Data curation, formal analysis; RZ: investigation, visualization; ZWC: formal analysis, investigation, writing—original draft; SYC: investigation, software, visualization; YXR: methodology, visualization; JJW: investigation, resources; TXS: investigation, visualization; ZYQ: Manuscript revision; XY and YZ: conceptualization, formal analysis, funding acquisition, investigation, project administration, supervision, writing; XD Zhu, JP and XD Zhang: project administration, supervision. All authors read and approved the final manuscript.

Funding
This work was supported by the Department of Science and Technology of Sichuan Province (23ZDYF2641), Health Commission of Sichuan Province (2023-118), Chengdu Science and Technology Program (2021-YF08-00107-GX), Department of Science and Technology of Chengdu (2023-GH02-00075-HZ), and the Fundamental Research Funds for the Central Universities (20826041G4189).

Availability of data and materials
All the data supporting the findings of this study are included in this manuscript.

Declarations

Ethics approval and consent to participate
The animal study was approved by the Ethical Committee of Sichuan University (KS2020308). All the animals were purchased from Laboratory Animal Center of Sichuan University. The animal experiment guidance from the ethical committee and the guide for care and use of laboratory animals of Sichuan University were followed during the whole experiment course.

Competing interests
The authors declare that they have no competing interests.

Author details
[1]Department of Orthopedics, West China Hospital, Orthopedic Research Institute, Sichuan University, Chengdu 610041, Sichuan, China. [2]National Engineering Research Center for Biomaterials, Sichuan University, Chengdu 610064, Sichuan, China. [3]Chengdu Integrated TCM and Western Medicine Hospital, Chengdu First People's Hospital, Chengdu 610041, Sichuan, China. [4]Department of Inspection, School of Medicine, Jiangsu University, Zhenjiang 212013, China. [5]State Key Laboratory of Oral Diseases and National Center for Stomatology and National Clinical Research Center for Oral Diseases, Department of Oral and Maxillofacial Surgery, West China Hospital of Stomatology, Sichuan University, Chengdu 610041, Sichuan, China. [6]State Key Laboratory of New Ceramics and Fine Processing, Key Laboratory of Advanced Materials of Ministry of Education, School of Materials Science and Engineering, Tsinghua University, Beijing 100084, China.

Received: 14 November 2023 Revised: 12 December 2023 Accepted: 14 December 2023
Published online: 19 December 2023

References

1. Haugen HJ, Lyngstadaas SP, Rossi F, Perale G. Bone grafts: which is the ideal biomaterial? J Clin Periodontol. 2019;46(Suppl 21):92.
2. Habibovic P. Strategic directions in osteoinduction and biomimetics. Tissue Eng Part A. 2017;23(23–24):1295.
3. Gillman CE, Jayasuriya AC. FDA-approved bone grafts and bone graft substitute devices in bone regeneration. Mater Sci Eng C Mater Biol Appl. 2021;130:112466.
4. Nauth A, Schemitsch E, Norris B, Nollin Z, Watson JT. Critical-size bone defects: is there a consensus for diagnosis and treatment? J Orthop Trauma. 2018;32(Suppl 1):7.
5. Roddy E, DeBaun MR, Daoud-Gray A, Yang YP, Gardner MJ. Treatment of critical-sized bone defects: clinical and tissue engineering perspectives. Eur J Orthop Surg Traumatol. 2018;28(3):351.
6. Yamada M, Egusa H. Current bone substitutes for implant dentistry. J Prosthodont Res. 2018;62(2):152.
7. Lichte P, Pape HC, Pufe T, Kobbe P, Fischer H. Scaffolds for bone healing: concepts, materials and evidence. Injury. 2011;42(6):569.
8. Ferretti C, Mattioli-Belmonte M. Periosteum derived stem cells for regenerative medicine proposals: boosting current knowledge. World J Stem Cells. 2014;6(3):266.
9. Nyman S, Gottlow J, Lindhe J, Karring T, Wennstrom J. New attachment formation by guided tissue regeneration. J Periodontal Res. 1987;22(3):252.
10. Buser D, Dula K, Belser U, Hirt HP, Berthold H. Localized ridge augmentation using guided bone regeneration. I. Surgical procedure in the maxilla. Int J Periodontics Restorative Dent. 1993;13(1):29.
11. Hutmacher D, Hürzeler MB, Schliephake H. A review of material properties of biodegradable and bioresorbable polymers and devices for GTR and GBR applications. Int J Oral Maxillofac Implants. 1996;11(5):667.
12. Wang Q, Xu JJ, Jin HM, Zheng WH, Zhang XL, Huang YX, Qian ZY. Artificial Periosteum in bone defect repair—a review. Chin Chem Lett. 2017;28(9):1801.
13. Calciolari E, Ravanetti F, Strange A, Mardas N, Bozec L, Cacchioli A, et al. Degradation pattern of a porcine collagen membrane in an in vivo model of guided bone regeneration. J Periodontal Res. 2018;53(3):430.
14. Chattopadhyay S, Raines RT. Review collagen-based biomaterials for wound healing. Biopolymers. 2014;101(8):821.
15. Oechsle AM, Häupler M, Weigel F, Gibis M, Kohlus R, Weiss J. Modulation of extruded collagen films by the addition of co-gelling proteins. J Food Eng. 2016;171:164–73.
16. Ber S, Torun Köse G, Hasirci V. Bone tissue engineering on patterned collagen films: an in vitro study. Biomaterials. 2005;26(14):1977.
17. Ma B, Han J, Zhang S, Liu F, Wang S, Duan J, et al. Hydroxyapatite nanobelt/polylactic acid Janus membrane with osteoinduction/barrier dual functions for precise bone defect repair. Acta Biomater. 2018;71:108.
18. Hiratsuka T, Uezono M, Takakuda K, Kikuchi M, Oshima S, Sato T, et al. Enhanced bone formation onto the bone surface using a hydroxyapatite/collagen bone-like nanocomposite. J Biomed Mater Res B Appl Biomater. 2020;108(2):391.
19. Yunoki S, Sugiura H, Ikoma T, Kondo E, Yasuda K, Tanaka J. Effects of increased collagen-matrix density on the mechanical properties and in vivo absorbability of hydroxyapatite-collagen composites as artificial bone materials. Biomed Mater. 2011;6(1):015012.
20. Liao SS, Cui FZ, Zhang W. Mineralized collagen based composite for bone tissue engineering. Zhongguo Yi Xue Ke Xue Yuan Xue Bao. 2003;25(1):36.
21. Liao SS, Cui FZ, Zhang W, Feng QL. Hierarchically biomimetic bone scaffold materials: nano-HA/collagen/PLA composite. J Biomed Mater Res B Appl Biomater. 2004;69(2):158.
22. Qiu ZY, Cui Y, Tao CS, Zhang ZQ, Tang PF, Mao KY, et al. Mineralized collagen: Rationale, current status, and clinical applications. Mater (Basel). 2015;8(8):4733.

23. Lian K, Lu H, Guo X, Cui F, Qiu Z, Xu S. The mineralized collagen for the reconstruction of intra-articular calcaneal fractures with trabecular defects. Biomatter. 2013;3(4):e27250.
24. Kou JM, Fu TY, Jia XJ, Hou JW, Gao C, Ma YZ. Clinical observations on repair of non-infected bone Nonunion by using mineralized collagen graft. J Biomaterials Tissue Eng. 2014;4:1107.
25. Nevins ML, Camelo M, Schupbach P, Kim DM, Camelo JM, Nevins M. Human histologic evaluation of mineralized collagen bone substitute and recombinant platelet-derived growth factor-BB to create bone for implant placement in extraction socket defects at 4 and 6 months: a case series. Int J Periodontics Restorative Dent. 2009;29(2):129.
26. Zhao YG, Zheng JC, Xiong Y, Wang HT, Yang SH, Sun XD, et al. Hierarchically engineered artificial lamellar bone with high strength and toughness. Small Struct. 2023;4:2200256.
27. Kikuchi M, Matsumoto HN, Yamada T, Koyama Y, Takakuda K, Tanaka J. Glutaraldehyde cross-linked hydroxyapatite/collagen self-organized nanocomposites. Biomaterials. 2004;25(1):63.
28. Landis WJ, Silver FH. Mineral deposition in the extracellular matrices of vertebrate tissues: identification of possible apatite nucleation sites on type I collagen. Cells Tissues Organs. 2009;189(1–4):20.
29. Zheng Z, Chen SY, Liu XD, Wang YJ, Bian Y, Feng B. A bioactive polymethylmethacrylate bone cement for prosthesis fixation in osteoporotic hip replacement Surgery. Mater Design. 2021;209:109966.
30. Ramos O, Reinas I, Silva S, Catalão J, Cerqueira M, Pereira R. Effect of whey protein purity and glycerol content upon physical properties of edible films manufactured therefrom. Food Hydrocolloids. 2013;30(1):110.
31. Yin SM, Zhang YZ, Zhang XX, Tao KY, Li GY. High-strength collagen/delphinidin film incorporated with Vaccinium oxycoccus pigment for active and intelligent food packaging. Collagen and Leather. 2023;5(1):1.
32. Liu F, Zhu KD, Ma YX, Yu Z, Chiou BS, Jia MW, et al. Collagen films with improved wet state mechanical properties by mineralization. Food Hydrocolloids. 2023;139:108579.
33. Bodde EW, Spauwen PH, Mikos AG, Jansen JA. Closing capacity of segmental radius defects in rabbits. J Biomed Mater Res A. 2008;85(1):206.
34. Zhao L, Zhao J, Wang S, Wang J, Liu J. Comparative study between tissue-engineered periosteum and structural allograft in rabbit critical-sized radial defect model. J Biomed Mater Res B Appl Biomater. 2011;97(1):1.
35. Geiger F, Bertram H, Berger I, Lorenz H, Wall O, Eckhardt C, et al. Vascular endothelial growth factor gene-activated matrix (VEGF165-GAM) enhances osteogenesis and angiogenesis in large segmental bone defects. J Bone Miner Res. 2005;20(11):2028.
36. Linde A, Alberius P, Dahlin C, Bjurstam K, Sundin Y. Osteopromotion: a soft-tissue exclusion principle using a membrane for bone healing and bone neogenesis. J Periodontol. 1993;64(Suppl 11):1116.
37. Schmitz JP, Schwartz Z, Hollinger JO, Boyan BD. Characterization of rat calvarial nonunion defects. Acta Anat (Basel). 1990;138(3):185.
38. Ueyama Y, Ishikawa K, Mano T, Koyama T, Nagatsuka H, Suzuki K, et al. Usefulness as guided bone regeneration membrane of the alginate membrane. Biomaterials. 2002;23(9):2027.
39. Ren YR, Fan L, Alkildani S, Liu L, Emmert S, Najman S, et al. Barrier membranes for guided bone regeneration (GBR): a focus on recent advances in Collagen Membranes. Int J Mol Sci. 2022;23:14987.
40. Walters MA, Leung YC, Blumenthal NC, LeGeros RZ, Konsker KA. A Raman and infrared spectroscopic investigation of biological hydroxyapatite. J Inorg Biochem. 1990;39(3):193.
41. Barth A. Infrared spectroscopy of proteins. Biochim Biophys Acta. 2007;1767(9):1073.
42. Dan WH, Chen YN, Dan NH, Zheng X, Wang L, Yang CK, et al. Multi-level collagen aggregates and their applications in biomedical applications. Int J Polym Anal Ch. 2019;24(8):667.
43. Payne JA, McCormick AV, Francis LF. A study of stress development in aqueous gelatin coatings. J Appl Polym. 1999;73(4):553.
44. Liu Y, Liu S, Luo D, Xue Z, Yang X, Gu L, et al. Hierarchically staggered nanostructure of mineralized collagen as a bone-grafting Scaffold. Adv Mater. 2019;31(2):e1807082.
45. Matsumoto T, Okazaki M, Inoue M, Hamada Y, Taira M, Takahashi J. Crystallinity and solubility characteristics of hydroxyapatite adsorbed amino acid. Biomaterials. 2002;23(10):2241.
46. Li JS, Li Y, Liu X, Zhang J, Zhang Y. Strategy to introduce an hydroxyapatite-keratin nanocomposite into a fibrous membrane for bone tissue engineering. J Mater Chem B. 2013;1(4):432.
47. Hadagalli K, Shenoy S, Shakya KR, Manjunath G, Tarafder K, Mandal S, et al. Effect of Fe3 + substitution on the structural modification and band structure modulated UV absorption of hydroxyapatite. Int J Appl Ceram Technol. 2021;18(2):332.
48. Zhang W, Yu J, Chang H. Two dimensional nanosheets as conductive, flexible elements in biomaterials. J Mater Chem B. 2015;3(25):4959.
49. Wu J, Liu F, Yu Z, Ma Y, Goff HD, Ma J, et al. Facile preparation of collagen fiber-glycerol-carboxymethyl cellulose composite film by immersing method. Carbohydr Polym. 2020;229:115429.
50. Zhao Y, Xiong Y, Zheng J, Kongling W, Chen J, Li C, et al. A multifaceted biomimetic periosteum with a lamellar architecture and osteogenic/angiogenic dual bioactivities. Biomater Sci. 2023;11(11):3878.
51. Charulatha V, Rajaram A. Influence of different crosslinking treatments on the physical properties of collagen membranes. Biomaterials. 2003;24(5):759.
52. Shi XD, Chen LW, Li SW, Sun XD, Cui FZ, Ma HM. The observed difference of RAW264.7 macrophage phenotype on mineralized collagen and hydroxyapatite. Biomed Mater. 2018;13(4):041001.
53. Jiang T, Heng S, Huang X, Zheng L, Kai D, Loh XJ, et al. Biomimetic poly(poly(ε-caprolactone)-polytetrahydrofuran urethane) based nanofibers enhanced chondrogenic differentiation and cartilage regeneration. J Biomed Nanotechnol. 2019;15(5):1005.
54. Xu SJ, Qiu ZY, Wu JJ, Kong XD, Weng XS, Cui FZ, et al. Osteogenic differentiation gene expression profiling of hMSCs on hydroxyapatite and mineralized collagen. Tissue Eng Part A. 2016;22(1–2):170.
55. Mariani E, Lisignoli G, Borzì RM, Pulsatelli L. Biomaterials: foreign bodies or tuners for the Immune response? Int J Mol Sci. 2019;20(3):636.
56. Vishwakarma A, Bhise NS, Evangelista MB, Rouwkema J, Dokmeci MR, Ghaemmaghami AM, et al. Engineering immunomodulatory biomaterials to tune the Inflammatory response. Trends Biotechnol. 2016;34(6):470.
57. Jiang L, Wang CG, Chee PL, Qu C, Fok AZ, Yong FH, et al. Strategies for lignin depolymerization and reconstruction towards functional polymers. Sustainable Energy & Fuels. 2023;7(13):2953.
58. Gretzer C, Emanuelsson L, Liljensten E, Thomsen P. The inflammatory cell influx and cytokines changes during transition from acute inflammation to fibrous repair around implanted materials. J Biomater Sci Polym Ed. 2006;17(6):669.
59. Lee HS, Stachelek SJ, Tomczyk N, Finley MJ, Composto RJ, Eckmann DM. Correlating macrophage morphology and cytokine production resulting from biomaterial contact. J Biomed Mater Res A. 2013;101(1):203.
60. Meng C, Liu K, Lv Z, Zhang Y, Li J, Luo X, et al. Inflammation and immunity gene expression profiling of macrophages on mineralized collagen. J Biomed Mater Res A. 2021;109(8):1328.
61. Sheikh Z, Brooks PJ, Barzilay O, Fine N, Glogauer M, Macrophages. Foreign body giant cells and their response to implantable biomaterials. Mater (Basel). 2015;8(9):5671.
62. Sanders JE, Stiles CE, Hayes CL. Tissue response to single-polymer fibers of varying diameters: evaluation of fibrous encapsulation and macrophage density. J Biomed Mater Res. 2000;52(1):231.
63. Fang JY, Yang Z, Han B. Switch of macrophage fusion competency by 3D matrices. Sci Rep. 2020;10(1):10348.
64. Guda T, Walker JA, Singleton BM, Hernandez JW, Son JS, Kim SG, et al. Guided bone regeneration in long-bone defects with a structural hydroxyapatite graft and collagen membrane. Tissue Eng Part A. 2013;19(17–18):1879.
65. Zhou DS, Zhao KB, Li Y, Cui FZ, Lee IS. Repair of segmental defects with nano-hydroxyapatite/collagen/PLA composite combined with mesenchymal stem cells. J Bioact Compat Polym. 2006;21(5):373.
66. Sathasivam T, Kai J, Sugiarto S, Yu Y, Soo DXY, Zhu Q, et al. Nano-Strategies for Lignin Biomaterials toward Cancer Therapy. Adv Healthc Mater. 2023;12(19):e2300024.
67. Leow Y, Shi JK, Liu W, Ni XP, Yew PYM, Liu S, et al. Design and development of multilayer cotton masks via machine learning. Mater Today Adv. 2021;12:100178.
68. Chen G, Lv Y. Matrix elasticity-modified scaffold loaded with SDF-1α improves the in situ regeneration of segmental bone defect in rabbit radius. Sci Rep. 2017;7(1):1672.

69. Liu FZ, Wang DW, Zhang YJ, Zhao Y, Sun XD, Li KY, et al. Comparison of rabbit rib defect regeneration with and without graft. J Mater Sci Mater Med. 2017;28(1):2.
70. Kai D, Jiang S, Low ZW, Loh XJ. Engineering highly stretchable lignin-based electrospun nanofibers for potential biomedical applications. J Mater Chem B. 2015;3(30):6194.

Publisher's Note